J Mater Sci (2008) 43:4022–4030
DOI 10.1007/s10853-007-2317-z

REES RAWLINGS FESTSCHRIFT

Crack resistance curve in glass matrix composite reinforced by long Nicalon® fibres

Ivo Dlouhy · Michal Kotoul · Tomas Vyslouzil · Zdenek Chlup · Aldo R. Boccaccini

Received: 2 July 2007 / Accepted: 13 November 2007 / Published online: 3 April 2008

Abstract Theoretical micromechanical analysis of bridged crack development at chevron-notch tip of three-point bend specimens has been applied to determine the crack resistance curve for a composite made of a glass matrix reinforced by continuous Nicalon® fibres. Fracture toughness (K_{IC}) values were determined using the chevron-notch technique at room temperature. The theoretical predictions were based on micromechanical analysis exploiting weight functions. Detailed FEM analysis using the ANSYS package was applied to determine numerically the weight functions for orthotropic materials. Appropriate bridging models for the theoretical prediction of the *R*-curve behaviour typical of the investigated composite were applied together with the weight functions. Experimental observations confirmed the theoretical calculations.

I. Dlouhy (✉) · Z. Chlup
Institute of Physics of Materials, ASCR, Zizkova 22,
61662 Brno, Czech Republic
e-mail: idlouhy@ipm.cz

M. Kotoul
Department of Solid Mechanics, Brno University of Technology,
Technicka 2, 616 69 Brno, Czech Republic
e-mail: kotoul@fme.vutbr.cz

T. Vyslouzil
Jan E. Purkyne University, Na okraji 1001,
400 96 Usti nad Labem, Czech Republic
e-mail: Vyslouzil@utrv.ujep.cz

A. R. Boccaccini
Department of Materials, Imperial College London,
London SW7 2BP, UK
e-mail: a.boccaccini@ic.ac.uk

Introduction

The development of flaw-tolerant fibre-reinforced ceramic and glass matrix composites in the last 20 years has resulted in a family of structural materials exhibiting quasi-ductile fracture behaviour in addition to other beneficial properties like oxidation resistance and high-temperature capability [1]. A fundamental requisite for these composites to be useful at high temperatures is the retention of a weak fibre/matrix interface, which is responsible for their flaw-tolerant behaviour [1–4].

In ceramics and glasses reinforced by ceramic fibres, elastic fibre bridging and fibre pull-out mechanisms mainly cause deformation energy dissipation and toughness increase. Both these toughening mechanisms increase to some extent behind the crack tip along the process zone wake [5, 6]. As a consequence, the crack growth resistance rises as the crack propagates and leaves the wake. The *R*-curve behaviour results from the presence of unbroken ligaments in the wake of the propagating crack, which exerts closure tractions along the crack surfaces. In these materials, it is difficult to define the intrinsic fracture toughness (e.g. K_{IC}) as a single material parameter due to the increasing crack growth resistance curve [5]. For further development of fibre-reinforced brittle matrix composites an exact method of fracture resistance quantification is needed, which is relevant also for the assessment of the possible structural degradation of the materials in service.

The most often used and standardized bend specimen geometries, the chevron-notch beam (CNB) and single edge notch beam (SENB), have been compared [7, 8]. Based on fractographic observations, differences in failure micromechanisms in both specimen geometries have been identified as shown schematically in Fig. 1. For the SENB

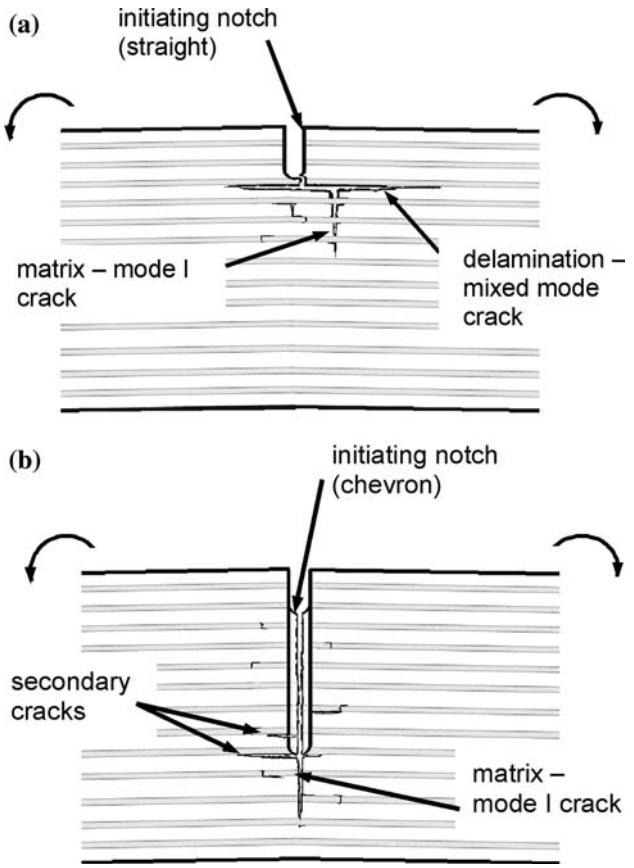

Fig. 1 Schematics of failure micromechanisms of composite for SENB specimen having a straight notch (**a**), and CNB specimen with chevron notch (**b**)

specimens (Fig. 1a) a mixed fracture mode was observed. Just below the notch root the propagation of minor cracks along the low-energy interfaces occurred. Fracture was not entirely confined to the propagation of a single crack. Mixed-mode crack caused increased deformation energy dissipation and thus the higher fracture toughness values when compared with the specimens with chevron notch [7]. For CNB specimens (Fig. 1b), the failure initiates in a relatively small volume near the chevron-notch tip and the condition for crack propagation, without premature localization near fibre/matrix interfaces, is more advantageous. For these specimens, the crack trajectory is controlled by the chevron-notch geometry keeping its plane, at least at the stage when data for fracture toughness determination are sampled. The crack-tip-driving force is higher than in case of SENB test. It is an important feature of the chevron-notch test that the conditions for unstable crack propagation are formed from the running crack. This is confirmed by the load-deflection curves, since the traces exhibit no sharp maximum.

The fracture initiation in CNB specimens is thus connected with a comparably lower probability, than for SENB specimen, that the major crack tip will meet a weak matrix–fibre interface and change the trajectory along the interface. In SENB specimens, due to a larger "process zone", some microcracks perpendicular to the major crack, i.e. along fibre–matrix interfaces, may be initiated. The total deformation energy will be thus higher and an overestimation of fracture toughness occurs. In addition, by using SENB specimens, it is not possible to obtain the crack resistance curve by unloading–loading technique and/or other approaches due to premature localization of the crack along the fibre/matrix interface. The chevron-notch technique is thus the only one capable of determining at least one single value from the crack resistance curve [7]. It seems that, combining the experimental determination of the fracture toughness value with the calculation of the crack resistance curve could lead to a clear description of the fracture behaviour of the investigated material and provide a means for its further optimization.

A disadvantage of the chevron-notch specimen geometry is the lack of an analytical solution for the stress intensity factor under different loading conditions. Bluhm's slice model [9] allows one to calculate the compliance and hence the geometry correction factor needed to calculate an averaged stress intensity factor for a CNB specimen using an available solution for a straight-through crack under the same loading conditions. To capture the effect of closure tractions acting along the bridged crack surfaces a weight-function-based approach was employed [9] to study the contribution of such tractions on the magnitude of the stress intensity at the crack tip in testing geometries with straight-through cracks. To apply a similar approach to the *R*-curves of macrocrack determined from chevron-notched specimen tests, a solution for the stress intensity factor resulting from the direct loading of the crack surfaces is needed. Bluhm's slice model relies on the knowledge of the so-called shear transfer coefficient that has to be determined by comparing experimental or numerical results with the analytical results which are based on an available analytical solution for a straight-through crack under the same loading. Since such a solution for a bridged crack with a general relationship between the bridging stresses and crack-opening displacement does not exist, Bluhm's method cannot be used to obtain the stress intensity factor resulting from the direct loading of the crack surfaces for a chevron-notched specimen.

However, a solution has been presented for an isotropic specimen using 3D FEM analysis [10, 11] where numerical results for the stress intensity caused by a unit load for a range of notch geometries were obtained. That procedure enabled to set up an analytical form of the weight function $h(\rho,a)$ by fitting numerical data by the function

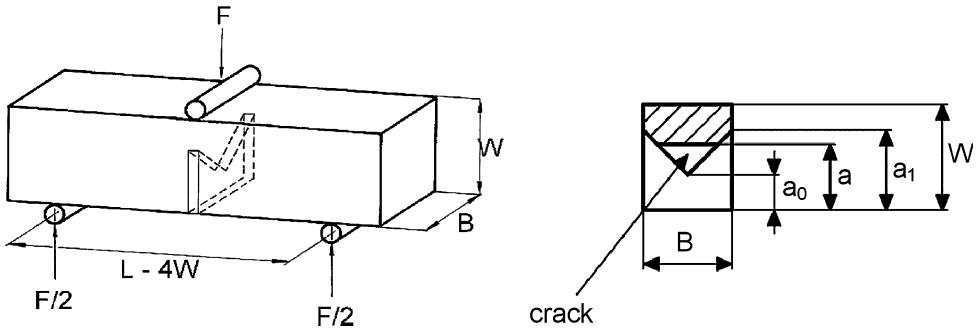

Fig. 2 Geometry of the chevron-notch three-point bend specimen

$$h(x,a) = \sqrt{\frac{2}{\pi(a-a_0)}}\frac{\rho}{\sqrt{1-\rho}} \times \left[1 + \sum_{(v,\mu)} \frac{A_{v,\mu}a^{\mu}}{(1-\alpha)^{3/2}}(1-\rho)^{v+1}\right], \quad (1)$$

where $\alpha = a/W$, $\rho = (x-a_0)/(a-a_0)$ are dimensional parameters, see Fig. 2, and the coefficients $A_{v,\mu}$ can be found in Ref. [11].

The most fundamental issues in the modelling of bridged crack growth and the overall specimen response are the bridging law, which determines the relationship between the bridging stresses and the crack-opening displacement, and an estimate of overall elastic properties of the composite. In our previous study [12] the overall elastic properties, deduced from the elastic properties of matrix and fibres under the assumption of perfect bonding at the fibre/matrix interface, and a simple bridging law, which assumes that fibres fracture at the crack mid-plane, led to a calculated three times lower specimen deflection in comparison to experimental data. This result suggests that the elastic moduli in the bending plane are reduced due to a limited transfer of load from the matrix to the fibres and due to matrix microcracking. Further, in accordance with experimental data, the fibres fracture within the matrix rather than at bridged faces of the matrix crack, thereby leading to frictionally constrained fibre pull-out.

A similar approach was adopted [13] to consider transversally isotropic specimens with the symmetry axis perpendicular to the notch plane. The main effort was exerted on modelling the bridged crack in the chevron-notched three-point bend specimen. The crack resistance curves and other characteristics have been calculated for selected values of Weibull modulus, strength of reinforcing fibres, and frictional shear stress, respectively.

The aim of the paper is the summarization of theoretical and experimental data on crack resistance behaviour obtained on borosilicate glass matrix composite reinforced with continuous SiC (Nicalon®) unidirectional fibres. The selected key results of the modelling and calculation procedures are analysed in connection with experimental data on the composite fracture behaviour.

Material and experimental techniques

A commercially produced unidirectional SiC Nicalon® (NL202) fibre-reinforced borosilicate (DURAN®) glass matrix composite was used for the investigation. Information on the composite constituents is given in Table 1. The composite was prepared by the sol–gel-slurry method [14]. The density of the composite was 2.4 g/cm^3 and its fibre volume fraction 0.4. Fairly regular fibre distribution and the absence of porosity were found by microstructural investigations, as shown in Fig. 3 [15]. The samples were received in the form of rectangular test bars of nominal dimensions 4.5 × 3.8 × 100 mm^3.

The chevron-notched beam (CNB) technique was employed for fracture toughness determination; the specimen geometry is shown in Fig. 2. Chevron notches with top angles of 90° were cut using a thin diamond wheel. A three-point bending test (with span of 16 mm) at a constant cross-head speed of 0.1 mm/min was employed. Traces of load versus deflection were recorded and the maximum

Table 1 Properties of the glass matrix, SiC fibres and composite [14, 15]

	Density (g/cm^3)	Young's modulus (GPa)	Poisson's ratio (–)	Thermal exp. coeff. (K^{-1})	Tensile strength (MPa)
DURAN® Glass	2.23	63	0.22	3.25 × 10^{-6}	60
Fibre SiC Nicalon®	2.55	198	0.20	3.0 × 10^{-6}	2750
Composite	2.40	118	0.21	3.1 × 10^{-6}	600–700

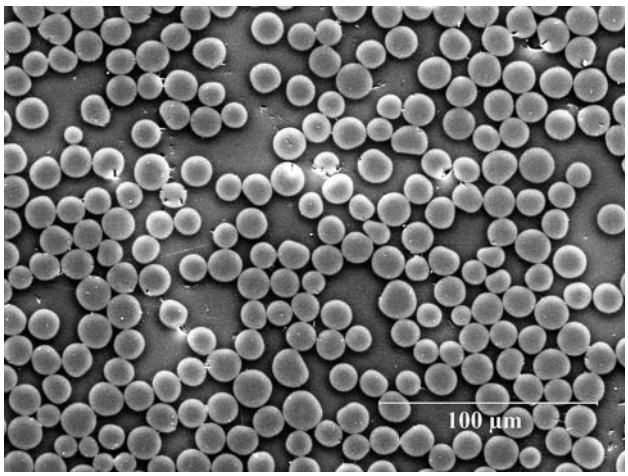

Fig. 3 Microstructure of the composite formed by borosilicate glass matrix reinforced by unidirectional fibres, section perpendicular to fibres, SEM

force was determined from each trace. The fracture toughness value was calculated from the maximum load (F_{max}) and the corresponding minimum value of geometrical compliance function (Y^*_{min}) using the equation

$$K_{IC} = \frac{F_{max}}{B\sqrt{W}} Y^*_{min}, \tag{2}$$

where B and W are dimensions of samples (Fig. 2). The calculation of the function Y^*_{min} for chevron-notch bend bars was based on the use of Bluhm's slice model [9]. The procedure used for the purposes of this investigation has been described elsewhere [16]. The chevron-notch depth a_0 was measured from optical micrographs of fractured specimens.

The acoustic emission technique (AE) was used during the tests. Traces of cumulative number of counts (AE events) were obtained in the same time scale as the load versus time plots. This technique allows for an accurate detection of the microcrack initiation at the chevron notch, which occurs when a sharp increase in the number of AE events is observed. Valid measurements for computing K_{IC} are those in which the increase of AE events coincides with the end of the linear part of the force versus time trace, as explained below.

An important supporting technique, scanning electron microscopy (SEM) was used to investigate fracture surfaces.

Finite element modelling and calculations

The 3D FEM mesh for the chevron-notched specimen was generated in the finite element system ANSYS as only one-quarter of the specimen, see Fig. 4. A combination of quadratic isoparametric and quarter-point elements is used.

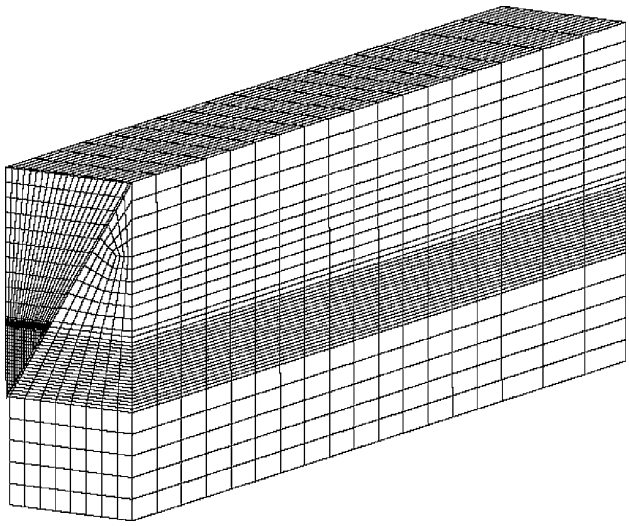

Fig. 4 3D FEM mesh used when modelling the chevron-notched specimen

To simulate the stress field singularity at the crack tip quarter-point elements in the shape of collapsed pentahedron with 15 nodes were used at the crack front. Further, a modification of this element was also used—namely pentahedron with 13 nodes.

The stress intensity factor was estimated from an extrapolation of crack-opening displacement. Due to the overall composite anisotropy the general relation was applied:

$$K = \lim_{r\to 0}\left(L\sqrt{\frac{2\pi}{r}}u\right), \tag{3}$$

where K is a vector with the stress intensity components K_{II}, K_I and K_{III} (in this order), $u = (u, v, w)$ is a vector with the displacement components on the crack faces and L is Barnett-Lothe's tensor. Supposing an orthotropic material the Barnett-Lothe's tensor was calculated [12] and led to following solution

$$K = -\lim_{r\to 0}\left(\frac{1}{a_{11}bc}\sqrt{\frac{2\pi}{r}}v\right). \tag{4}$$

The bridging stress gives rise to the bridging stress intensity factor, K_{Ibr}, and as a result, the local stress intensity $K_{Itip} = K_{Iapp1} - K_{Ibr}$ acting in the very crack tip is lower than the remote applied stress intensity K_{Iapp1}.

During the stable crack growth the local stress intensity K_{Itip} is kept equal to the critical orthotropic stress intensity factor K_{ICM} for matrix cracking in the direction perpendicular to the direction of fibres, which follows as [17]:

$$K_{ICM} = K_m\sqrt{\frac{AE_1(1-v_m^2)}{E_m(1-v^2)}(1-c_f)}, \tag{5}$$

where K_m is the fracture toughness of the matrix, v_m and v denote Poisson's ratio of the matrix and the composite, respectively. A is a dimensionless factor that characterizes the orthotropy. According to Tada et al. [18], quoting results of Sih et al. [19], the value of this factor can be calculated using Eq. $A = (1 - v_{23}^2)/CE_1$, which, for the composite considered, gives the value $A \cong 0.92$. The factor $(1 - c_f)$ accounts for the reduction in length of the edge of the matrix crack due to the presence of the aligned fibres.

The local stress intensity factor K_{tip} can be calculated by means of the weight function $h(x, a)$ [9] from:

$$K_{Itip} = K_{Iappl} - K_{Ibr} = \int_0^a h(x,a)\left[\sigma_{appl}(x) - \sigma_{br}(x)\right]dx, \tag{6}$$

where a is the crack length, $\sigma_{app1}(x)$ denotes the traction along the prospective crack plane in uncracked component and the weight function $h(x, a)$ is, in the current configuration, the stress intensity factor $K(a)$ resulting from the line load acting along a line behind the crack tip. To obtain numerically the weight function from FEM calculations, a similar approach as presented in Ref. [11] was adopted. The line load P was applied to the crack face in such a way that $P/b(x)$, where $b(x)$ is the local width of the wake of the crack, and x is defined as in Fig. 2, was kept constant. By applying such a line load to the crack surfaces over the region $a_0 < x < a$, the value of the weight function at an arbitrary position x was calculated from

$$h(x,a) = \frac{K(a)}{P/b(x)}. \tag{7}$$

The total displacements of the crack surface $\delta = \delta_{app1} + \delta_{br}$ (note that $\delta_{br} < 0$) can be derived from prior knowledge of the weight function from the integral equation:

$$\delta(x) = -a_{11}bc\int_x^a h(x,a') \times \left\{\int_0^{a'} h(x',a')\left[\sigma_{appl}(x') - \sigma_{br}(\delta(x'))dx'\right]\right\}da'. \tag{8}$$

The stress intensity factors describing the R-curve behaviour were obtained by the following manner: (i) the total crack-opening displacements have to be found from the solution of the integral Eq. 8, (ii) the bridging stress distribution $\sigma_{br}(x) = \sigma_{br}(\delta(x))$ is thus obtained and the associated bridging stress intensity factor K_{Ibr} results from Eq. 6 as

$$K_{Ibr} = \int_0^a h(x,a)\sigma_{br}(x)dx, \tag{9}$$

(iii) finally, the crack-tip stress intensity factor $K_{Itip} = K_{Iapp1} - K_{Ibr}$ is calculated and set equal to the critical orthotropic stress intensity factor K_{ICM}

$$K_{Itip} = K_{ICM}. \tag{10}$$

Instead of extracting an analytical form of the weight function from FEM results and solving Eqs. 8–10, a modified approach was chosen [13]. This approach is based on numerical data obtained from the FEM analysis, which were used as an input for a recurrent procedure designed in the system MAPLE to solve numerically the problem described. The procedure requires considering two sets of loading in the FEM modelling [13]:

(1) The specimen was loaded by unit force F_0 causing three-point bending, see Fig. 2, and $v_{app1} = \delta_{app1}/2$ was calculated for a range of crack-notch geometries.
(2) The specimen was loaded by the line force P_0 uniformly distributed along the local width of the wake of the crack $b(x)$ with $P_0/b(x) = 1$ and acting at the distance $a - x$ from the crack tip. $v_{br} = \delta_{br}/2$ was calculated for a wide range of crack-notch geometries [13]. In both calculations it was assumed that the stress intensity factor K was constant along the crack front, and its magnitude was taken as the average over those calculated at each position along the crack front. The results were recorded into files which were used as input files for recurrent calculations performed in the system MAPLE [13]. The aim of recurrent calculations in the system MAPLE was to find the loading force F and the total displacement of the upper crack face under the condition that $K_{Itip} = K_{ICM}$.

Fracture performance of the composite

To introduce the composite fracture behaviour, Fig. 5 shows a typical load deflection trace obtained during the three-point bend test of the chevron-notched specimen. The acoustic emission technique indicated that individual microfracture events started at about one-third of the maximum load, as demonstrated by a beginning of smooth increase (marked by arrow (i) in Fig. 5) in the cumulative number of AE events. It is the stage where slope change on the load-deflection curve occurred being caused by increased presence of microcracks in the glass matrix. The change in slope is marked by the dashed linear regression lines 1 and 2. The analysis of deflection traces indicated that crack developed at about two-third of maximum load at the chevron-notch tip (marked by arrow (ii) in Fig. 5),

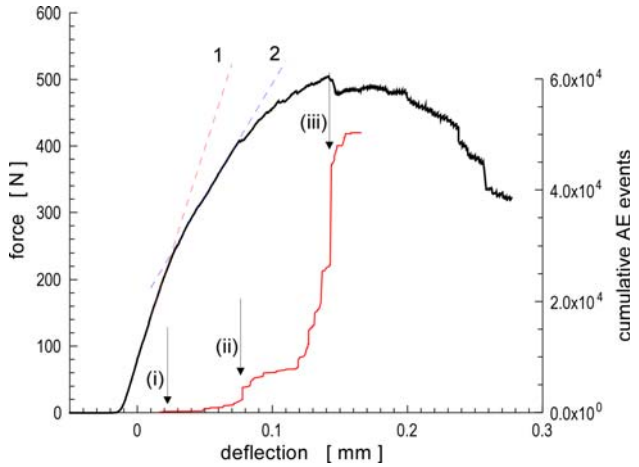

Fig. 5 Load-deflection trace obtained during bend test of chevron-notch specimen at room temperature

and it propagated in a controlled manner up to maximum load after which unstable fracture occurred (arrow (iii)).

At two-third level of the maximum load rapid increase in the AE signal occurred (marked by arrow (ii) in Fig. 5). This increase of AE events and similar increase in later stages of specimen loading are so high that crack propagation through the glass matrix and fibre/matrix debonding and fracture are thought to be responsible for this significant effect, as discussed in a paper [20]. A detailed analysis of the trace in Fig. 5 indicates that deviation from linearity occurs at this stage (arrow (ii)). An increase in the number of AE events observed at the end of the increasing part of the load-deflection traces (arrow (iii) in Fig. 5) indicates that the actual cracks have been developed at the chevron-notch tip. In these cases, the measurements of K_{IC} can be taken as valid, since the unstable fracture (at maximum force) occurs from a propagating crack perpendicular to the fibre axis [20].

The typical fracture surface morphology showing well-developed fibre pull-out mechanism can be observed in the SEM image of Fig. 6a. Compared to SENB specimen with straight notch a very regular distribution of fibres can be seen. Fracture surface morphology of separate fibres broken during tensile tests usually exhibit three stages of micro-crack development, i.e. mirror, mist and hackle [1, 21]. This was not the case when fibres cracked after extensive pull-out, however [21]. This difference in fracture surface morphology can be assigned to good interfacial bond between matrix and fibre and to the constraint imposed by the rigid surrounding matrix which leads to fracture nucleation inside the fibre and development of the first stage of fracture, i.e. mirror formation. In chevron-notched specimen fracture surfaces, only some fibres exhibited the fracture morphology typical of free fibres under tensile loads (see the fibre in the bottom left area in Fig. 6b).

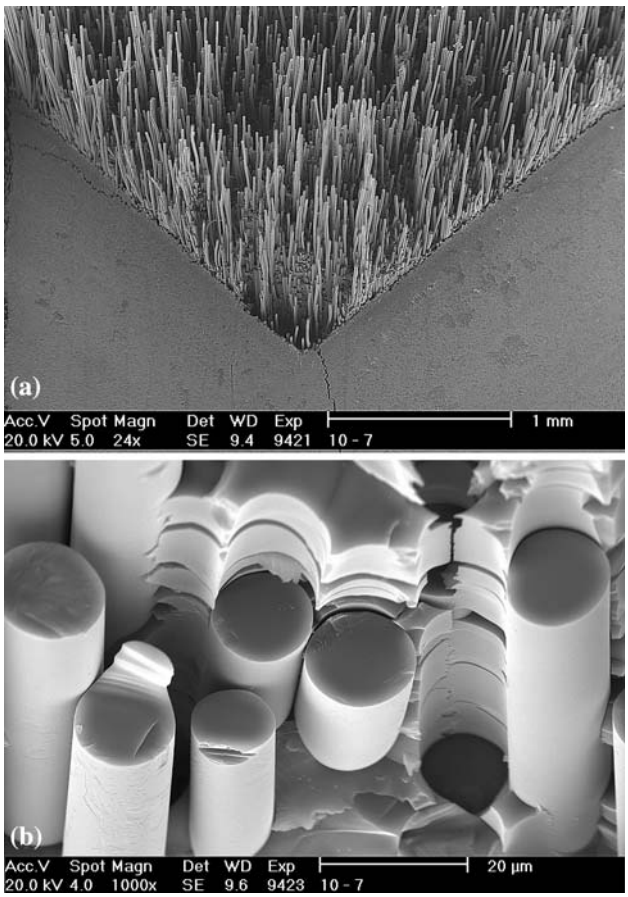

Fig. 6 Typical fracture surface morphology of the chevron-notch specimens (**a**) and detail of fracture surface of fibres after pull-out, SEM (**b**)

Results of fracture toughness determination for a set of specimens of the same geometry are shown in a rank probability diagram in Fig. 7. The individual values are spread in intervals from 23.6 to 26.6 MPa $m^{1/2}$.

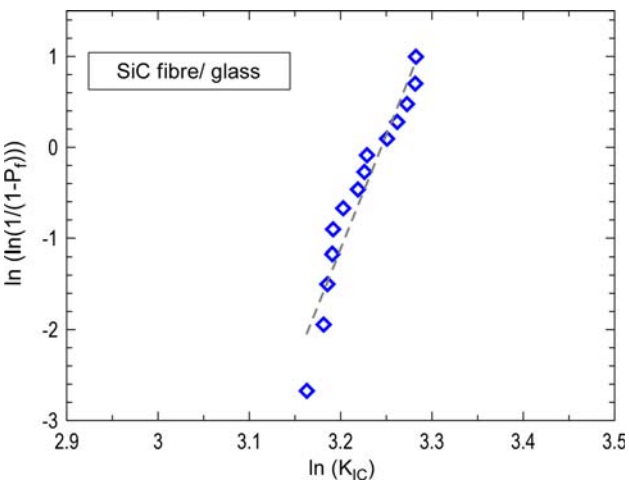

Fig. 7 Rank probability diagram of fracture toughness values determined by means of chevron-notch technique

Numerical results

The calculations were carried out considering the value of the critical orthotropic stress intensity factor of the matrix $K_{ICM} = 0.7$ MPa m$^{1/2}$ [8]. The specimen width was $W = 4.5$ mm and the notch depth was $a_0 = 1.8$ mm. The main point of the analysis was to determine theoretically the R-curve for the specified material and specimen geometry and to predict unstable fracture. Based upon the recurrent calculations [12] it was possible to find out how the applied force F has to be increased in order to keep the crack propagation in stable regime and, correspondingly, to calculate the appropriate stress intensity factor

$$K_{\mathrm{Iappl}}(F, \Delta a) = K_{\mathrm{IC}} + K_{\mathrm{Ibr}}(F, \Delta a). \tag{11}$$

The values of the stress intensity in Eq. 11 can be identified with the crack growth resistance K_{IR} and plotted as a function of crack length a. The stress intensity factor for different constant loading forces, K_{Iapp1}, can be plotted as a function of crack length a as well. Unstable fracture occurs at a specified point of the K_{IR}–Δa curve, called K_{Iinst}, where the corresponding K_{Iapp1} curve is tangential to the K_{IR} curve:

$$K_{\mathrm{Iappl}} = K_{\mathrm{IR}}, \left.\frac{\delta K_{\mathrm{Iappl}}}{\delta a}\right|_{\mathrm{F=const}} = \frac{dK_{\mathrm{IR}}}{da}. \tag{12}$$

Selected results are presented in Figs. 8 and 9, where the effect of the characteristic fibre strength σ_{0f}, interface frictional shear stress τ and the Weibull modulus m is also demonstrated.

In Fig. 8 the effect of the characteristic fibre strength σ_{0f} is demonstrated while keeping the interface frictional shear stress and the Weibull modulus constant. All calculations were performed for the microcracking zone present as well as for microcracking suppressed. Figure 8 shows three crack growth resistance curves K_{IR} calculated for three values of the characteristic fibre strength σ_{0f}, while the other parameters are kept constant as indicated in the figure legend. It can be seen that K_{Iapp1} curves are tangential to the K_{IR} curves at points $K_{\mathrm{Iinst}} \in (25;35)$ MPa m$^{1/2}$ for the microcrack zone present, and at points $K_{\mathrm{Iinst}} \in (30;40)$ MPa m$^{1/2}$ for microcracking suppressed. Corresponding values of the critical loading force F_{crit} range from 285 N to 353 N for the microcracked composite and from 278 N to 358 N for microcracking suppressed.

In a similar fashion Fig. 9 shows the effect of Weibull modulus while keeping the fibre strength σ_{0f} and frictional shear stress constant (Fig. 9a) and the effect of the interface frictional shear stress τ while keeping the characteristic fibre strength σ_{0f} and the Weibull modulus constant (Fig. 9b). Both figures supply the crack resistance curves for the microcracking zone present, as this mechanism has been proved by the change in the slope of linear parts of load-deflection traces.

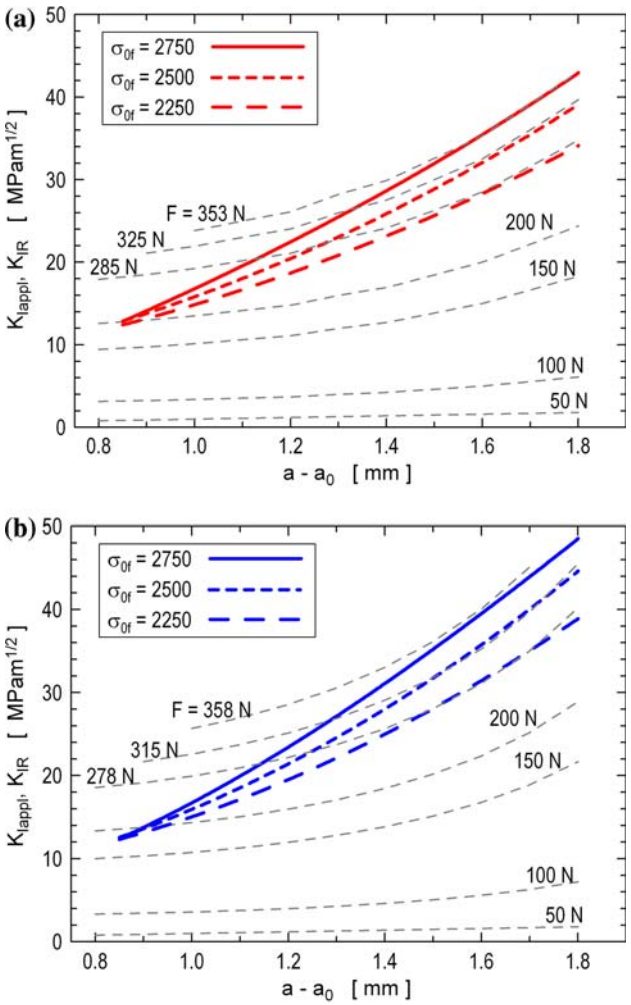

Fig. 8 Crack growth resistance curves K_{IR}–Δa for several values of the characteristic fibre strength σ_{0f}, supposing $\tau = 6$ MPa, $m = 5.3$, and development of K_{Iappl} corresponding to different applied loads for (**a**) saturated microcracked zone being considered, (**b**) microcracking suppressed

With decreasing value of the Weibull modulus (Fig. 9a) the ordinate of the tangent point corresponding to the initiation of unstable fracture increases from $K_{\mathrm{Iinst}} \approx 35$ MPa m$^{1/2}$ for $m = 5.3$ to $K_{\mathrm{Iinst}} \approx 45$ MPa m$^{1/2}$ for $m = 3.5$ for the microcracked composite present. For microcracking suppressed the values corresponding to unstable fracture initiation are on the level from $K_{\mathrm{Iinst}} \approx 35$ MPa m$^{1/2}$ $K_{\mathrm{Iinst}} \approx 40$ MPa m$^{1/2}$ for $m = 5.3$ to $K_{\mathrm{Iinst}} \approx 57$ MPa m$^{1/2}$ for $m = 3.5$ [13]. The corresponding values of the critical loading force F_{crit} range from 353 N to 433 N for the microcracked composite. The effect of the Weibull modulus m upon the K_{IR} curve clearly follows from the bridging law. Apparently, with decreasing m, the average distance from the

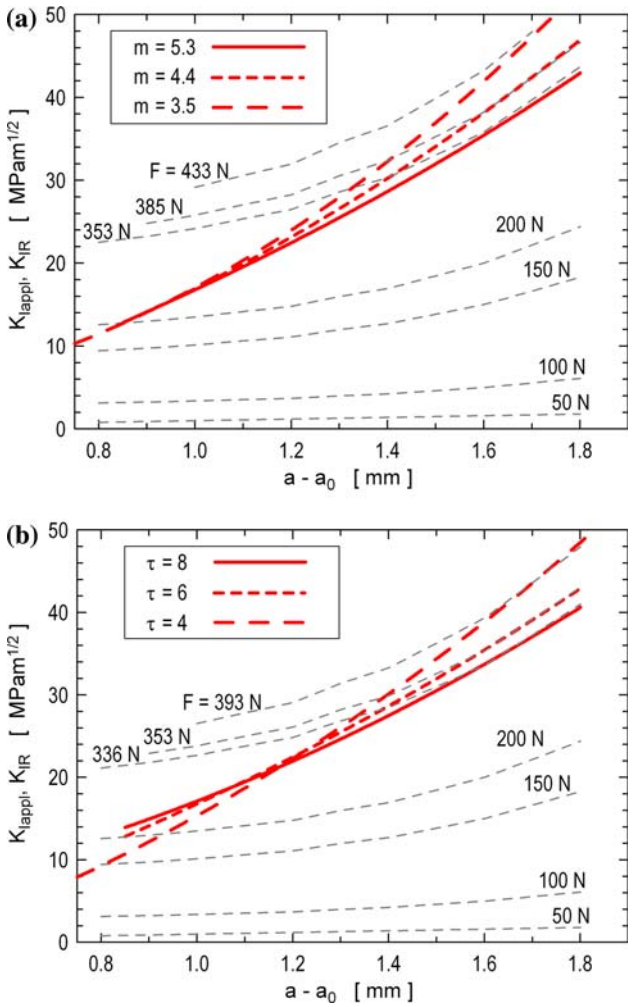

Fig. 9 Crack growth resistance curves K_{IR}–Δa for several values of the Weibull modulus m, supposing σ_{0f} = 2750 MPa, τ = 6 MPa (**a**), and for several values of the frictional shear stress τ, supposing σ_{0f} = 2750 MPa, m = 5.3 (**b**), both with developments of K_{Iappl}; saturated microcracked zone being considered

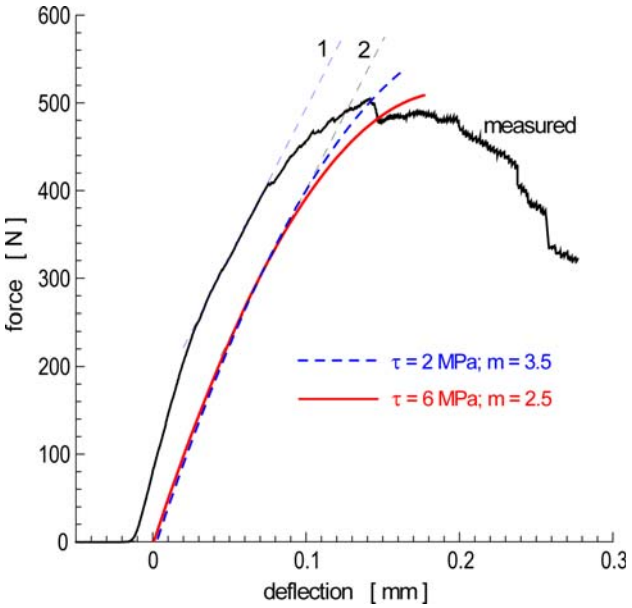

Fig. 10 Calculated load-deflection curves for two combinations of frictional shear stress τ and Weibull modulus m, the characteristic fibre strength being the same (saturated microcracked zone being supposed), and comparison with experimentally determined curve

fibre failure position to the crack plane increases, thus promoting the stress transferred by the broken fibres.

Figure 9b demonstrates the effect of the varying frictional shear stress τ upon crack growth resistance curves. Though the higher frictional shear stress leads to the higher bridging stress at lower crack face displacement, the average distance from the fibre failure position to the crack plane decreases with increasing τ because the tensile stress in the fibres builds up faster and, as a consequence, the bridged zone length decreases and the resulting bridging effect is reduced. With decreasing value of the frictional shear stress the ordinate of the tangent point corresponding to the inception of unstable fracture increases from $K_{Iinst} \approx 30$ MPa m$^{1/2}$ for τ = 8MPa to $K_{Iinst} \approx 40$ MPa m$^{1/2}$ for τ = 4MPa. Corresponding values of the critical loading force F_{crit} range from 336 N to 493 N.

To confirm the numerical results the force-deflection curves have been calculated. The calculation has been carried out for the tested geometry of CNB specimen. Arising from literature data [22, 23] two levels of frictional stress have been applied with the characteristic fibre strength being on the level of σ_{0f} = 2750 MPa. The calculated curves of loading force, F, on the specimen deflection, p, have been plotted and compared with the measured one, see Fig. 10. Quite good agreement has been found, e.g. in the linear elastic part corresponding to matrix microcracking the slopes of linear regression curves (1 and 2) are the same for the measured and calculated curve up to departure from the linearity. The calculations of the load-deflection curves are physically meaningful up to the maximum loading force. Beyond this point, fracture becomes unstable and a quasi-static analysis does not hold any longer.

Conclusion

The work has demonstrated that the chevron-notched specimen technique can be a reliable method to assess fracture behaviour in brittle matrix composites reinforced by continuous fibres which are typical by increasing crack resistance curve. The fracture toughness (K_{IC}) values determined using the chevron-notched specimen technique on the composite investigated (having a mean value of 24.6 MPa m$^{1/2}$) are comparable to data in the literature obtained in similar materials [24]. In comparison with other

methods, the chevron-notch technique offers high accuracy for K_{IC} determination because more reproducible conditions for crack initiation are assured.

Crack resistance curves for crack growth in the chevron-notched three-point bending specimen made of the glass matrix composite reinforced by SiC Nicalon® fibres were computed using a weight-function approach supplemented by the bridging model. This model follows from the assumption of large fibre slip lengths adjacent to the crack faces, whereas the fibre strength follows the Weibull statistics. As the side product of *R*-curve computations a relationship between the loading force and the specimen deflection was obtained for a range of micromechanical parameters such as the frictional shear stress, the characteristic fibre strength and the Weibull modulus describing a distribution in the fibre tensile strength values. Theoretical predictions of critical load and stress intensity factor at the start of unstable fracture were found to be in acceptable agreement with experimental data. The developed computational analysis seems to provide an efficient tool for designing new brittle matrix composites reinforced by long brittle fibres.

Acknowledgements The research was supported by the Czech Science Foundation under grant numbers 106/05/0495 and 106/06/0724 is gratefully acknowledged.

References

1. Chawla KK (1993) Ceramic matrix composites. Chapman and Hall, London
2. Boccaccini AR, Rawlings RD (2002) Glass Technol 43C:191
3. Kim HS, Yong JA, Rawlings RD et al (1991) Mater Sci Tech Ser 7:155
4. Rawlings RD (2001) Brittleness—a tough problem. In: Pashley DW (ed) Imperial College inaugural lectures in materials science and materials engineering. Imperial College Press, London, pp 153–197, ISBN: 1-8609-4106-0
5. Akatsu T, Yasuda E, Sakai M (1996) Fract Mech 11:245
6. Thouless MD, Evans AG (1988) Acta Metall 36:517
7. Dlouhy I, Boccaccini AR (2001) Scripta Materialia 44:531
8. Boccaccini AR, Rawlings RD, Dlouhy I (2003) Mat Sci Eng A Struct 347:102
9. Bluhm JI (1975) Eng Fract Mech 7:593
10. Fett T, Munz D, Seidel J, Stech M, Rödel J (1996) J Am Ceram Soc 79:1189
11. Sarrafi-Nour GR, Coyle TW, Fett T (1998) Eng Fract Mech 59:439
12. Kotoul M, Vyslouzil T, Dlouhy I (2005) In: Aliabadi MH et al (eds) Proceedings of advances in fracture and damage mechanics IV. EC Ltd, UK, pp 217
13. Kotoul M, Vyslouzil T, Boccaccini AR, Dlouhy I Theoretical and experimental study of crack growth in glass matrix composite reinforced by long SiC fibres, Theoretical and applied fracture mechanics. doi:10.1016/j.tafmec.2007.11.001
14. Pannhorst W et al (1990) Ceram Eng Sci Proc 11:947
15. Dlouhy I, Reinisch M, Boccaccini AR (2002) Fracture toughness and work of fracture of SiC fibre reinforced glass matrix composite, Fracture mechanics of ceramics, crack/microstructure interaction, R-curve behaviour. Kluwer, pp 203
16. Dlouhy I, Holzmann M, Man J, Valka L (1994) Metall Mater 32:3
17. Budiansky B, Cui YL (1994) J Mech Phys Solids 42:l
18. Tada H, Paris P, Irwin GR (1985) The stress analysis of cracks handbook. Del Research, St Louis
19. Sih GC, Paris PC, Irwin GR (1965) Int J Fract Mech 1:189
20. Boccaccini AR, Kern H, Dlouhy I (2001) Mater Sci Eng A308:111
21. Dlouhý I, Chlup Z (2005) Key Eng Mater 290:167
22. Kastritseas C, Smith PA, Yeomans JA (2005) Comp Sci Technol 65:1880
23. Chiang YCh (2001) Comp Sci Technol 61:1743
24. Brennan JJ, Prewo KM (1982) J Mater Sci 17:2371.